Aggregation of the nucleic acid–binding protein TDP-43 occurs via distinct routes that are coordinated with stress granule formation

Received for publication, October 18, 2018, and in revised form, January 8, 2019 Published, Papers in Press, January 10, 2019, DOI 10.1074/jbc.RA118.006351

Youjun Chen and Todd J. Cohen[1]

From the Department of Neurology, University of North Carolina Neuroscience Center, University of North Carolina, Chapel Hill, North Carolina 27599

Edited by Paul E. Fraser

TAR DNA-binding protein 43 (TDP-43) is a nucleic acid–binding protein, and its aggregation represents the defining pathology in amyotrophic lateral sclerosis (ALS) and related proteinopathies. Recent studies implicate cytoplasmic stress granules (SGs) as hubs that may facilitate TDP-43 aggregation. Here, using cellular fractionation, biochemical analyses, and histological assays, we show that TDP-43 targeted to the cytoplasm has multiple fates. Whereas a TDP-43 subpopulation is indeed recruited to SGs, mature aggregated TDP-43, produced with aggregate-prone TDP-43 variants or exposure to oxidative stress, generates distinct TDP-43 inclusions that are surprisingly devoid of SGs. Consistent with this observation, we found that SG components are predominantly excluded from TDP-43 pathology in motor neurons from individuals with ALS. We generated *de novo* SGs by expressing the fragile X protein (FMRP) and found that rather than directly engaging TDP-43 aggregates, SGs can sequester the proteostasis factor histone deacetylase 6 (HDAC6) and thereby impede TDP-43 clearance from cells. These findings indicate that SGs form distinct cytoplasmic structures that can indirectly enhance TDP-43 aggregation. Therapeutic approaches that inhibit SG formation may therefore be effective at suppressing TDP-43–mediated toxicity in patients with ALS and related TDP-43 proteinopathies.

TDP-43 is an RNA-binding protein that forms the major pathology in amyotrophic lateral sclerosis (ALS),[2] frontotemporal lobar degeneration (FTLD-TDP), and related proteinopathies (1). In addition, missense mutations in the *TARDBP* gene have been identified as pathogenic for familial ALS and FTLD-TDP (2, 3). Over the last few years, questions have emerged regarding pathologic mechanisms by which TDP-43 aggregation is initiated, including the role of post-translational modifications in driving aberrant TDP-43 accumulation (4–7). Although C-terminal TDP-43 phosphorylation (on serine residues 403/404 and 409/410) is an excellent marker of disease pathology, in some instances TDP-43 phosphorylation suppressed rather than promoted aggregation (8), prompting us to consider alternative modifications that impact TDP-43.

Recently, we discovered that TDP-43 is subject to reversible lysine acetylation at residues Lys-145 and Lys-192 within the RNA-binding domains (RNA recognition motifs). Either acetylation-mimicking TDP-43 mutations or fully acetylated TDP-43 (achieved with the acetyltransferase CBP/p300) led to insoluble, hyperphosphorylated, and ubiquitinated TDP-43 aggregates that were readily engaged by autophagy and ubiquitin-proteasome pathways but not efficiently cleared and accumulated as pathological inclusions (4, 9). Consistent with a role for this modification in disease, acetylated TDP-43 was detected in ALS patient spinal cord harboring full-length TDP-43 but was not present in FTLD-TDP brain containing mostly cleaved C-terminal TDP-43 fragments that lack the Lys-145 residue (10). We proposed that aberrantly acetylated TDP-43 triggers its aggregation in a similar manner to genetic *TARDBP* mutations, some of which also reside within the RNA recognition motif domains and potentially modulate critical interactions between TDP-43 and target mRNA (11, 12).

TDP-43 acetylation was most prominent when TDP-43 was targeted to the cytoplasm, prompting us to consider its role in cytoplasmic mRNA triage. Stress granules (SGs) are membrane-less organelles with a cytoprotective role, representing active sites of RNA triage in response to environmental insults (13, 14). Studies have shown that TDP-43 is recruited to SGs in response to a variety of stressors (15–20). Our previous study showed that TDP-43 localizes to SGs in a manner that depends on the toxic nature of the environmental insult (21). What remains unclear is the relevance of TDP-43 localization to SGs and whether these structures may act as putative harbingers of disease pathology. This issue has important clinical implications since persistent SGs were proposed to initiate ALS pathogenesis (22–24).

The RNA-binding protein FMRP, implicated in fragile X syndrome, is an excellent marker of SGs that co-localizes with TDP-43 during stress (21). FMRP was shown to bind TDP-43, co-regulate shared downstream mRNA targets, alter TDP-43 solubility, and modulate TDP-43 toxicity in a *Drosophila* model (25–28). Thus, FMRP may control TDP-43 function and aggre-

This work was supported by National Institutes of Health Grants R00 NS080985 (to T. J. C.) and R01NS105981 (to T. J. C.). The authors declare that they have no conflicts of interest with the contents of this article. The content is solely the responsibility of the authors and does not necessarily represent the official views of the National Institutes of Health.

This article contains Figs. S1–S3.

[1] To whom correspondence should be addressed: Dept. of Neurology, University of North Carolina, Chapel Hill, NC 27599. Tel.: 919-966-3759; Fax: 919-843-4576; E-mail: toddcohen@neurology.unc.edu.

[2] The abbreviations used are: ALS, amyotrophic lateral sclerosis; FTD, frontotemporal dementia; FTLD, frontotemporal lobar degeneration; SG, stress granule; HDAC, histone deacetylase; IHC, immunohistochemistry; NLS, nuclear localization sequence; RIPA, radioimmune precipitation assay.

gate-induced toxicity. However, the link between FMRP, SGs, and TDP-43 pathology has not been fully investigated, because it remains challenging to reproduce robust full-length TDP-43 pathology needed to address the interplay between these factors.

Here, we provide evidence that SGs and mature TDP-43 aggregates are distinct yet coordinated cytoplasmic entities. Although TDP-43 becomes partly integrated into SGs, more aggregate-prone TDP-43 species, generated by pathogenic modifications or exposure to sublethal stress conditions, are surprisingly devoid of SGs. In support of these observations, limited SG pathology was observed in ALS patient motor neurons. We propose that pathological TDP-43 undergoes a conformational transition that disrupts its interaction with SGs, leading to the evolution of a distinct ALS inclusion pathology.

Results

Cytoplasmic TDP-43 forms SG-associated and non–SG-associated structures

A small pool of nuclear TDP-43 relocalizes to SGs upon exposure to environmental stressors (17, 29). However, under pathological conditions, TDP-43 preferentially accumulates in cytoplasmic inclusions. To determine whether cytoplasmic TDP-43 is recruited to SGs, we expressed TDP-43 lacking a nuclear localization sequence (TDP-43–ΔNLS) or a comparable variant containing aggregate-prone acetylation-mimic substitutions at residues Lys-145 and Lys-192 (TDP-43–ΔNLS–2KQ), the latter of which generates very robust TDP-43 inclusions that more closely resemble ALS pathology (4). Although cytoplasmic TDP-43 targeting alone did not cause significant accumulation within SGs (Fig. 1*A*), the more aggregate-prone TDP-43 mutant showed enhanced SG localization detected with multiple SG markers including FMRP and TIAR (Fig. 1, *B* and *C*, see *cyan arrowheads* marking SGs). Aggregate-prone TDP-43–ΔNLS–2KQ also occasionally formed distinct amorphous inclusions with minimal SG co-localization (Fig. 1, *C* and *D*, see *magenta arrowheads* marking large inclusions). In contrast to SG markers, Hsp70 strongly labeled the TDP-43 inclusions (Fig. 1*D*), consistent with the recruitment of chaperones as a TDP-43 clearance mechanism (9).

To further assess the interplay between TDP-43 and SGs, we induced aggregation of cytoplasmic targeted TDP-43 (TDP-43–ΔNLS) using a sublethal arsenite exposure (0.25 mM for 1 h), previously shown to promote TDP-43 cysteine cross-linking and rapid TDP-43 aggregation (21). Similar to acetylation-mimic inclusions, arsenite-induced aggregation produced amorphous inclusions that did not co-localize with FMRP-immunoreactive SGs (Fig. 1*E*). An even more pronounced separation of these compartments was observed with TDP-43–ΔNLS–2KQ (Fig. 1*F*). Quantification of these results showed a significant reduction in TDP-43 recruitment to SGs upon stress exposure (Fig. 1*G*). Thus, although cytoplasmic TDP-43 can integrate into SGs, it also rapidly aggregates into a spectrum of SG-negative inclusions that are more reminiscent of the hallmark pathology seen in ALS patients.

SG localization in ALS spinal cord

To assess SG localization patterns in diseased motor neurons, we analyzed human postmortem spinal cord tissue from ALS patients. A previous report suggested that some SG components were recruited to inclusions in ALS and FTD patient brain or spinal cord (29). Given the minimal overlap of FMRP with aggregate-prone TDP-43 inclusions *in vitro* (Fig. 1), we analyzed total FMRP and P-FMRP immunoreactivity (Fig. 2). We note that P-FMRP is also a robust SG marker in cultured cells (Fig. S1). Immunohistochemistry (IHC) showed that FMRP and P-FMRP were diffusely cytoplasmic in ALS motor neurons and did not show patterns that resembled or correlated with TDP-43 pathology (Fig. 2*A*, see *magenta arrowheads* marking TDP-43 pathology). Confirming this observation, double labeling showed abundant skein-like, filamentous, and spherical TDP-43 inclusions with minimal FMRP or P-FMRP co-localization (Fig. 2, *B* and *C*).

Double-labeling experiments were also performed with antibodies detecting TIA-1 and TIAR (primary SG nucleators), which also showed limited co-localization with mature TDP-43 inclusions (Fig. 2, *D* and *E*). We note that although TIA-1 was closely juxtaposed to TDP-43 inclusions in a subset of motor neurons, it did not directly co-localize with TDP-43 (Fig. 2*D*). Similarly, whereas TIAR showed a somewhat stippled cytoplasmic localization pattern in motor neurons, these foci did not co-localize with aggregated TDP-43 inclusions (Fig. 2*E*, *inset*). Overall, our results in cultured cells and ALS spinal cord support the notion that mature TDP-43 pathology undergoes a morphological transition that is quite distinct from physiological SG assemblies.

De novo FMRP granules are distinct from mature TDP-43 pathology

We next sought to generate *de novo* SGs to ask whether SGs formed in the absence of cellular stress are sufficient to recruit TDP-43. We used a low-level FMRP overexpression paradigm in which the human FMR1 promoter drives expression of GFP-tagged FMRP (30). In this system, ectopically expressed FMRP generates granules that closely resemble stress-induced SGs (31, 32). We found that *de novo* FMRP granules were sufficient to recruit endogenous TDP-43, as detected with either N- or C-terminal TDP-43 antibodies (5) (Fig. 3, *A* and *B*, see *cyan arrowheads* marking SGs), suggesting that SG-localized TDP-43 is predominantly full-length rather than truncated. Cytoplasmic TDP-43–ΔNLS (Fig. 3*C*) and more prominently TDP-43–ΔNLS–2KQ (Fig. 3*D*) were both recruited to FMRP–GFP granules in transfected QBI-293 cells or primary cortical neurons (Fig. 3*E*). Aggregate-prone TDP-43–ΔNLS–2KQ formed inclusions that showed little overlap with FMRP–GFP granules. Indeed, we confirmed that SG-negative inclusions contained hyperphosphorylated pathological TDP-43 (Fig. 3*F*). The addition of arsenite further dissociated FMRP–GFP granules from TDP-43 inclusions (Fig. 3, *G* and *H*; see also quantification in Fig. 3*I*).

An aggregation time course was performed to evaluate the dynamics of FMRP granules and TDP-43 inclusions in response to arsenite (Fig. 4). In the absence of stress, TDP-43–ΔNLS is

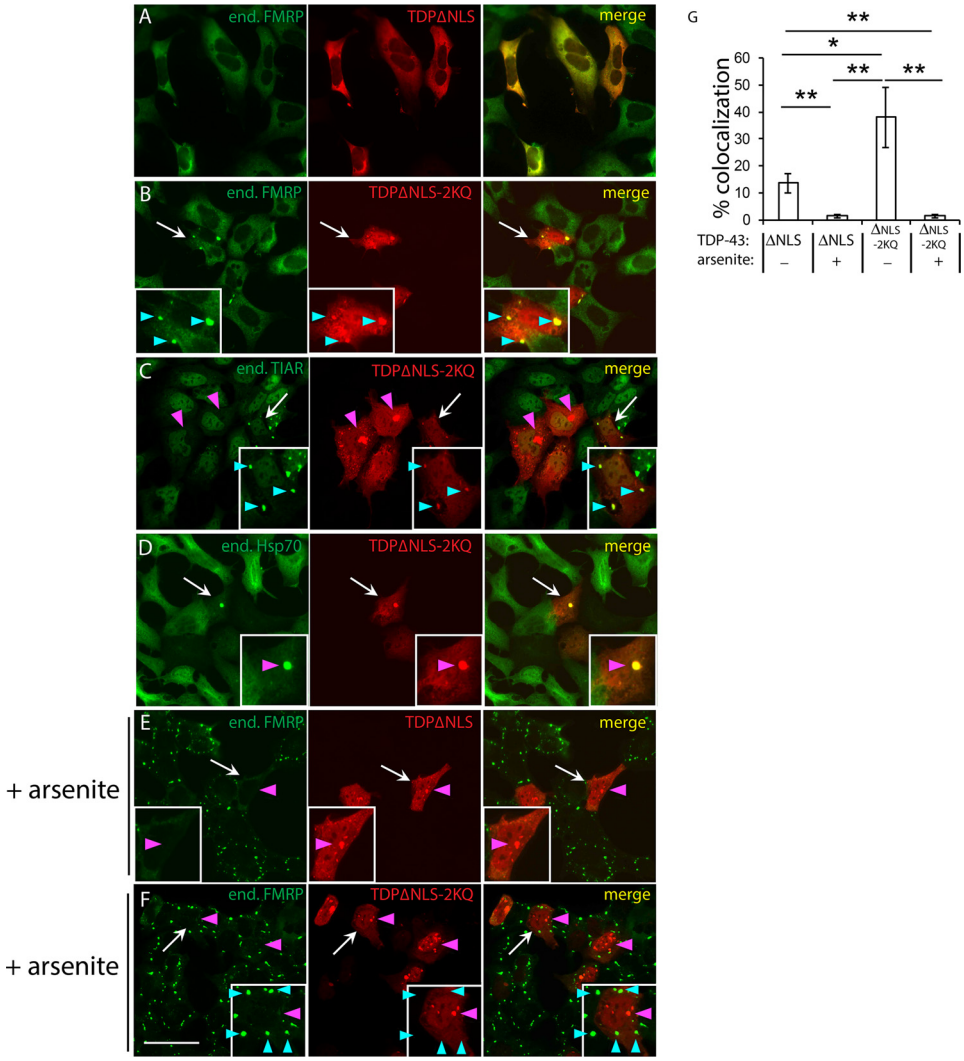

Figure 1. TDP-43 has multiple fates leading to SGs or cytoplasmic inclusions. *A–F*, QBI-293 cells were transfected with full-length cytoplasmic targeted TDP-43 constructs containing two mutated nuclear localization sequences (NLS1 and NLS2) yielding TDP-43–ΔNLS. This construct harbors mutations spanning ^{82}KRK^{84} and ^{95}KVKR^{98} motifs: K82A/R83A/K84A/K95A/K97A/R98A. The comparable TDP-43–ΔNLS–2KQ mutant harbors two additional lysine-to-glutamine mutations (K145Q/K192Q) that were shown to mimic cytoplasmic acetylation of TDP-43 and thereby enhance TDP-43 aggregation propensity. Transfected cells were left untreated (*A–D*) or exposed to 0.25 mM sodium arsenite (*E* and *F*) for 1 h at 37 °C in complete medium and subsequently fixed and analyzed by immunofluorescence microscopy using antibodies detecting Myc-tagged TDP-43 in combination with FMRP (*A*, *B*, *E*, and *F*), TIAR (*C*), or Hsp70 (*D*). *Scale bar*, 50 μm. *White arrows* highlight cells that are magnified in the *inset*, *cyan arrowheads* highlight SGs, and *magenta arrowheads* highlight TDP-43 inclusions. *G*, co-localization of FMRP granules in TDP-43 transfected cells was quantified using >100 granules from $n = 10$ fields per condition ($n = 3$ independent experiments) using ImageJ software. The values represent percentages of total FMRP granules that co-localize with ectopically expressed Myc-tagged TDP-43. *Error bars* indicate S.E., and *p* values were calculated by Student's *t* test. ***, $p < 0.001$; **, $p < 0.01$; *, $p < 0.05$. TDP-43–ΔNLS showed less granule formation compared with the acetylation mimic TDP-43–ΔNLS–2KQ. Arsenite-induced inclusion formation reduced the co-localization of TDP-43 with SGs.

primarily punctate and diffusely cytoplasmic, but within 30 min of arsenite exposure, small TDP-43 foci begin to emerge, many of which co-localized with FMRP (Fig. 4, see *cyan arrowheads* for 30-min time point). Other similarly sized TDP-43 aggregates that remained FMRP-negative instead coalesced into phosphorylated P409/410-positive TDP-43 inclusions (Fig. 4, see *magenta arrowheads* for 30-min time point). By 60 min, more robust perinuclear and phosphorylated inclusions began to accumulate that were almost completely devoid of FMRP (Fig. 4, see *magenta arrowheads* for 60-min time point marking phospho–TDP-43 inclusions). These results support a distinct morphological transition from TDP-43–positive cytoplasmic SGs to mature aggregated inclusions.

SGs indirectly modulate TDP-43 aggregation propensity

To further interrogate the interplay between TDP-43 and SGs, we examined whether TDP-43 inclusions influenced FMRP. We found that cytoplasmic TDP-43 aggregates partially co-localized with phosphorylated FMRP at Ser-499 (Fig. S1, *A* and *B*), a marker of stalled polyribosomes and translational repression (31, 33), but which had not previously been linked to SGs or TDP-43 aggregation. We therefore asked whether TDP-43 aggregates altered FMRP phosphorylation status. TDP-43 constructs were co-expressed with FMRP–GFP followed by FMRP immunoprecipitation and incubation with or without λ-phosphatase to identify phosphorylated FMRP protein bands. The more aggregate-prone cytoplasmic TDP-43–

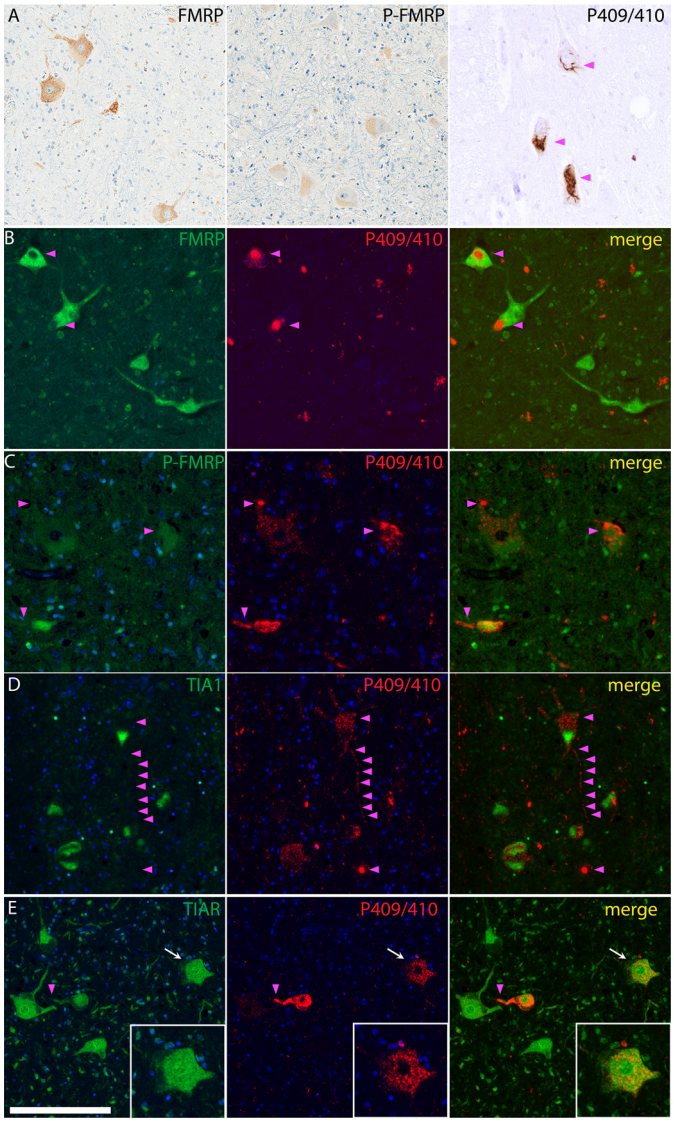

Figure 2. Stress granules and ALS spinal cord inclusions form distinct cytoplasmic structures. *A*, IHC was performed on lumbar spinal cord sections from sporadic ALS cases harboring TDP-43 pathology. *B–E*, TDP-43 inclusions were labeled with phosphorylated (*P409/410*) TDP-43 antibodies (*red*), and stress granules were marked by FMRP (*B*), P-FMRP (*C*), TIA-1 (*D*), or TIAR (*E*), antibodies (*green*). All ALS cases displayed spinal cord pathology, as assessed by phosphorylated 409/410 immunoreactivity. There was minimal co-localization of SG markers with either skein-like, round, or filamentous TDP-43 aggregates (see merged panels). The specificity of all SG antibodies was validated by SG immunoreactivity in arsenite-treated cells. Secondary evaluation of antibody specificity was tested by positive immunoreactivity in cells overexpressing FMRP, TIA-1, and/or TIAR. *Scale bar*, 200 μm. *White arrows* highlight neurons that are magnified in *insets*, and *magenta arrowheads* highlight TDP-43 inclusions.

ΔNLS–2KQ increased FMRP phosphorylation, which was abrogated by phosphatase treatment (Fig. S1*C*). Thus, aggregate-prone TDP-43 species can regulate SG components.

We next addressed the central issue of whether FMRP granules influence TDP-43 aggregation propensity. Given the spatial separation of SGs from mature TDP-43 inclusions, we considered the possibility that recruitment of key proteostasis factors to FMRP granules, and hence their sequestration or depletion from the cytoplasm, might indirectly enhance TDP-43 aggregation. Among the factors known to be enriched in SGs, we focused on the deacetylase HDAC6, previously shown to regulate SG dynamics (34) and also mediate autophagy-dependent processing of diverse aggregates including TDP-43 (35, 36). We first examined whether endogenous HDAC6 was physically sequestered within ectopically generated FMRP granules. Indeed, FMRP granules recruited a pool of endogenous cytoplasmic HDAC6 (Fig. 5*A*, see *cyan arrowheads* highlighting HDAC6-positive granules).

To clarify whether HDAC6 sequestration to granules and therefore loss of its normal function could exacerbate TDP-43 aggregation, biochemical fractionation studies were performed to evaluate TDP-43 solubility. We fractionated TDP-43 aggregates after pharmacological inhibition with the HDAC6 selective inhibitor tubastatin A (TBST) and observed a significant increase in insoluble phosphorylated TDP-43 by immunoblotting (Fig. 5*B*, compare *lanes 1–3* with *lanes 4–6*). Strikingly, a similar increase in insoluble TDP-43 was observed in the presence of FMRP–GFP alone (Fig. 5*B*, compare *lanes 1–3* with *lanes 7–9*). The effect of FMRP–GFP in driving TDP-43 aggregation occurred despite the fact that FMRP granules and TDP-43 inclusions did not co-localize. In addition, the FMRP-mediated increase in TDP-43 aggregation was not further exacerbated when combined with TBST, suggesting that *de novo* FMRP granules and HDAC6 inhibition may coordinately increase TDP-43 aggregation (Fig. 5*B*, compare *lanes 4–12*, and see full quantification in Fig. 5*C*). We note that inhibition of HDAC6 in the presence of FMRP granules did however significantly increase TDP-43 inclusion size, consistent with a role for HDAC6 in TDP-43 clearance (Fig. 5, *D* and *E*) (35, 37, 38). Similar to our analysis in cultured cell lines, inhibition of HDAC6 in primary cortical neurons that contained stress-induced SGs was sufficient to enhance cytoplasmic TDP-43 accumulation (Fig. S2, see *white arrows* marking cytoplasmic TDP-43 puncta).

To demonstrate that restoring HDAC6 expression can alleviate SG-induced TDP-43 aggregation, control or WT HDAC6 expression vectors were co-transfected with FMRP, and cell lysates were fractionated to evaluate TDP-43 aggregation. A reduction of aberrant TDP-43 species was observed, particularly with the insoluble pool of TDP-43, whereas soluble TDP-43 levels were not appreciably affected (Fig. 5*F*, compare *lanes 1–3* with *lanes 4–6*). By employing a panel of C-terminal HDAC6 deletion constructs, we observed that suppression of TDP-43 aggregation did not require the extreme C-terminal ubiquitin-binding domain (BUZ domain) shown to mediate association with polyubiquitinated substrates (35). However, the HDAC6 1–840 construct lacking the additional SE14 domain, a region known to interact with diverse aggregate-prone proteins including Tau and SOD1 (39, 40), was no longer capable of clearing TDP-43 aggregates (Fig. 5*F*, compare *lanes 4–6* with *lanes 10–12*) despite its localization to TDP-43 inclusions (Fig. S3). Quantification of these results showed that WT HDAC6, but not HDAC6 1–840, significantly suppressed TDP-43 aggregation by ~3-fold (Fig. 5*G*). The suppression of TDP-43 aggregation was similarly observed with overexpression of Hsp70 (Fig. S3). Thus, SGs can indirectly enhance TDP-43 aggregation and facilitate the formation of disease-linked inclusions by depleting critical proteostasis regulators such as HDAC6.

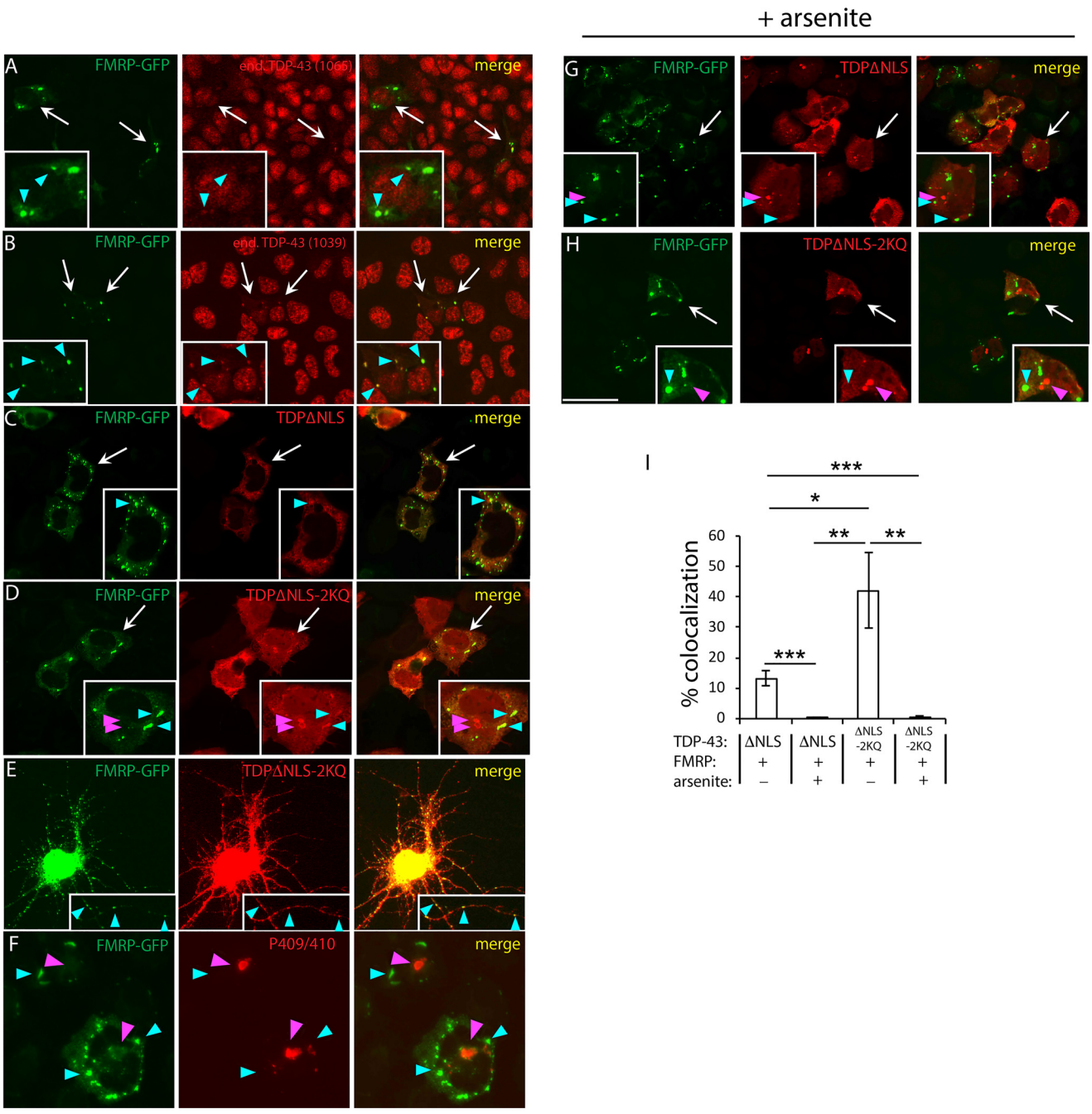

Figure 3. *De novo* FMRP granules recruit endogenous TDP-43 but are distinct from mature TDP-43 inclusions. *A* and *B*, cells expressing FMRP–GFP (driven by the human FMR1 promoter) were double-labeled to detect endogenous TDP-43 using polyclonal anti-TDP-43 1065 (*A*) or 1039 (*B*). Anti–TDP-43–1039 detects the extreme C terminus of TDP-43, whereas anti–TDP-43–1065 detects the extreme N terminus. *De novo* FMRP granules were sufficient to recruit endogenous full-length TDP-43. *C–H*, cytoplasmic-targeted TDP-43–ΔNLS or TDP-43–ΔNLS–2KQ mutants were co-expressed with FMRP–GFP in QBI-293 cells (*C*, *D*, and *F–H*) or transfected primary cortical neurons (*E*), which resulted in *de novo* production of cytoplasmic FMRP granules. Spherical FMRP–GFP granules were spatially distinct from the amorphous TDP-43 inclusions generated by the TDP-43–ΔNLS–2KQ mutant (*D* and *F*) or in response to arsenite (*G* and *H*). *Scale bar*, 50 μm. *White arrows* highlight individual cells that are magnified in the *insets*, *cyan arrowheads* highlight FMRP granules, and *magenta arrowheads* highlight TDP-43 inclusions. *I*, quantification of the percentage of FMRP-positive granules that co-localized with TDP-43 was determined using ImageJ software, as described in the Fig. 1 legend. *Error bars* indicate S.E., and *p* values were calculated by Student's *t* test. ***, $p < 0.001$; **, $p < 0.01$; *, $p < 0.05$.

Discussion

In this study, we explored the interplay between TDP-43 pathology and SGs. Reproducing full-length TDP-43 pathology similar to that seen in ALS/FTD has been challenging. To overcome this, we used genetic and pharmacological approaches to generate mature TDP-43 aggregates that are more reflective of ALS pathology as a means to interrogate the relationship between these cytoplasmic structures.

Our motivation came from an emerging hypothesis that SGs may become coopted during ALS pathogenesis, acting as a critical hub that initiates pathological TDP-43 aggregation (23). Indeed, we and others suggested that chronic SG recruitment of

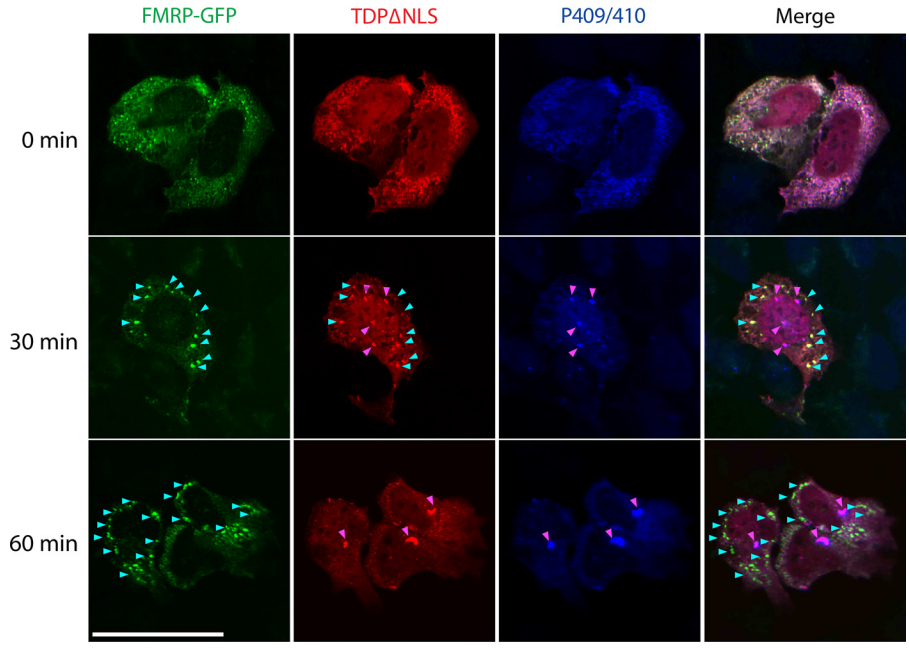

Figure 4. TDP-43 aggregates undergo a dynamic transition from cytoplasmic granules to mature inclusions. Cells co-expressing cytoplasmic TDP-43 (TDP-43–ΔNLS) and FMRP–GFP were treated with 0.25 mM arsenite for up to 60 min, followed by fixation and triple labeling to detect FMRP granules (*green*), total TDP-43 (*red*), and pathological phospho-TDP-43–positive (*P409/410*) inclusions (*blue*) by confocal microscopy. *Cyan arrowheads* highlight FMRP granules, and *magenta arrowheads* highlight mature TDP-43 inclusions. We note a gradual stress-dependent transition in TDP-43 morphology from granular SG-associated puncta to mature inclusions by ~30 min, which corresponded with the emergence of phosphorylated TDP-43 (*P409/410*) inclusions and minimal co-localization with FMRP–GFP. *Scale bar*, 20 μm.

TDP-43 could eventually produce hallmark TDP-43 pathology in individuals with ALS/FTD spectrum disorders (41). However, we found that SGs and mature TDP-43 aggregates are separable. Reversible SGs retain their spherical morphology, whereas mature TDP-43 aggregates (induced by either aggregate-prone TDP-43 modifications or acute oxidative stress) tend to coalesce and form larger aggregated structures containing amorphous, filamentous, and/or skein-like morphology. Interestingly, a similar phenomenon was observed with the ALS-associated Fus protein, in which the authors noted a clear morphological distinction between cytoplasmic Fus granules and larger Fus aggregates, with the latter being more similar to inclusion pathology in ALS–FUS patients (42).

SG formation is thought to occur as a consequence of liquid-liquid phase transitions, a biochemical property of several RNA-binding proteins now implicated in ALS and FTD (43–46). We speculate that TDP-43 pathology may emerge through a complex series of conformational changes (*e.g.* stress-mediated), post-translational modifications (*e.g.* phosphorylation and acetylation), and the presence of any genetic variants/mutations (*e.g.* ALS-linked mutations), all of which could modify its liquid-like properties to enhance TDP-43 aggregation. How might SGs influence these parameters? First, SGs may act as a short-lived intermediate that seed and/or modify stable TDP-43 aggregates that dissociate from SGs. Indeed, we show that stress-induced or *de novo* produced SGs co-localize with cytoplasmic TDP-43 but then show limited co-localization as mature TDP-43 aggregates begin to emerge (Figs. 1–3), despite the fact that both entities (SGs and mature aggregates) co-exist in individual cells. Our findings are consistent with those of McGurk *et al.* (47), who recently proposed that SGs might protect TDP-43 from aberrant phosphorylation and aggregation. Second, small pools of aggregated TDP-43 may emerge through a completely SG-independent mechanism. The rare detection of SGs (at least those SGs marked by FMRP, TIA-1, or TIAR) that co-localize with TDP-43 in ALS motor neurons (Fig. 2) indicates that SGs may not necessarily be required to directly precipitate TDP-43 pathology, at least using the SG markers and conditions employed in this study. Consistent with our histology findings, two recent studies showed no evidence for TIA-1 recruitment to TDP-43 inclusions in ALS patients with or without missense mutations in the *TIA-1* gene (48, 49). Lastly, one can envision a model whereby SGs indirectly promote TDP-43 pathology that is consistent with our data showing sequestration of HDAC6 (and potentially many other proteostasis factors) to cytoplasmic RNA granules (Fig. 5).

Our prior study showed that TDP-43 acetylation regulates mRNA binding, because both the Lys-145 and Lys-192 target lysines are in close proximity to the nucleic acid– binding interface (4). Thus, TDP-43 acetylation and reduced RNA binding may regulate TDP-43's ability to incorporate into SGs and direct TDP-43 toward an alternative and perhaps more aggregated fate. Consistent with this possibility, oxidative stress, which promotes TDP-43 acetylation and dissociation from target mRNAs, similarly promotes TDP-43 aggregation and dissociation from SGs (4). Future RNA-Seq approaches could help identify the full scope of TDP-43 targets that are sequestered in SGs, whose expression may become deregulated by aberrant TDP-43 acetylation.

We identified HDAC6 as a component of FMRP granules (Fig. 5*A*), which is consistent with a prior report linking HDAC6 to SG dynamics (34). We also showed that blocking HDAC6 led to an increase in the insoluble TDP-43 pool (Fig. 5*B*), suggesting that HDAC6 inhibitors may in fact exacerbate

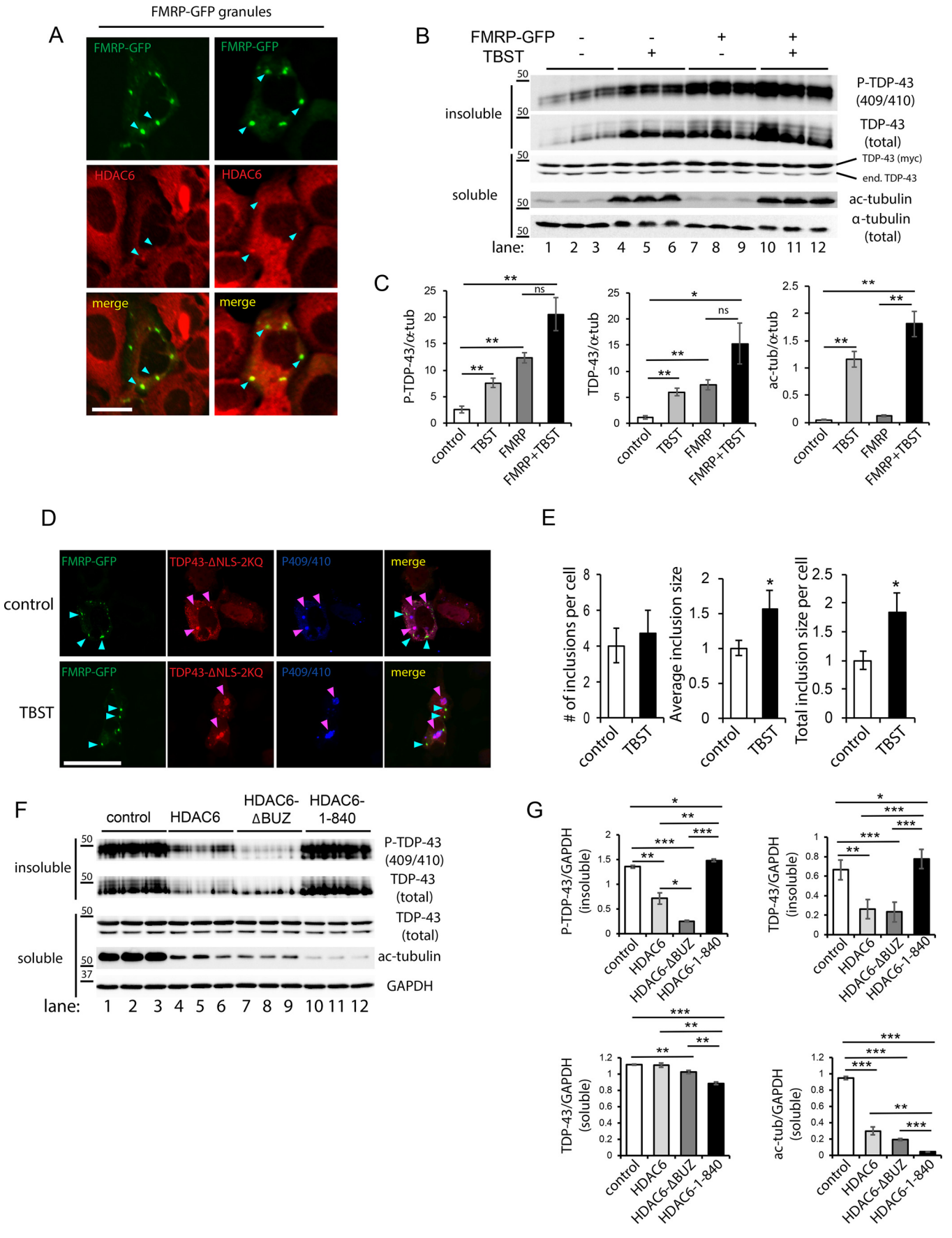
A
FMRP-GFP granules
FMRP-GFP
FMRP-GFP
HDAC6
HDAC6
merge
merge
B
FMRP-GFP
TBST
insoluble
soluble
P-TDP-43 (409/410)
TDP-43 (total)
TDP-43 (myc)
end. TDP-43
ac-tubulin
α-tubulin (total)
lane: 1 2 3 4 5 6 7 8 9 10 11 12
C
P-TDP-43/α-tub
TDP-43/α-tub
ac-tub/α-tub
control
TBST
FMRP
FMRP+TBST
D
control
TBST
FMRP-GFP
TDP43-ΔNLS-2KQ
P409/410
merge
E
# of inclusions per cell
Average inclusion size
Total inclusion size per cell
F
control
HDAC6
HDAC6-ΔBUZ
HDAC6-1-840
insoluble
soluble
P-TDP-43 (409/410)
TDP-43 (total)
TDP-43 (total)
ac-tubulin
GAPDH
lane: 1 2 3 4 5 6 7 8 9 10 11 12
G
P-TDP-43/GAPDH (insoluble)
TDP-43/GAPDH (insoluble)
TDP-43/GAPDH (soluble)
ac-tub/GAPDH (soluble)

TDP-43 aggregation within these cellular contexts. Although HDAC6 inhibitors have shown some potential as neuroprotective agents in ALS models (50, 51), it is worth noting that HDAC6 function is critical for maintaining proteostasis, potentially by trafficking protein aggregates via microtubule-bound dynein motors and delivering bound cargo to the autophagy-lysosomal machinery for degradation (35). Indeed, several studies have suggested a protective role for HDAC6 in suppressing toxicity (36, 38). Considering that HDAC6 inhibition can increase protein aggregation, increase the levels of damaged mitochondria via impaired mitophagy (52), and prevent efficient autophagic-lysosomal fusion (36), these data may warrant a re-evaluation of the therapeutic utility of HDAC6 inhibitors. In fact, it may be critical to evaluate HDAC6 inhibitor efficacy at specific stages of disease progression or define the impact of these compounds on specific cell-types (*e.g.* neurons and glia) in the central nervous system.

The paradoxical effects of HDAC6 inhibitors could also reflect the diversity of cytosolic HDAC6 substrates. Future efforts are needed to distinguish the role of HDAC6 as a regulator of tubulin acetylation *versus* nontubulin substrates including, for example, the actin remodeling machinery (*e.g.* actin and cortactin) (53), a variety of MT-associated factors (*e.g.* Tau, MAP2, and MAP4) (54), and heat shock proteins whose activities are controlled by reversible lysine acetylation (*e.g.* Hsp70 and Hsp90) (55, 56). Such insights could pave the way toward targeted approaches to modulate HDAC6 activity in a more substrate-selective manner.

Experimental procedures

Plasmids and cell culture

QBI-293 cells (MP Biomedicals) are commercially available and maintained according to standard protocol. The protocols followed in our animal studies were approved by the University of North Carolina Institutional Animal Care and Use Committee (approval no. 17-049). Primary cortical neurons were isolated from CD1 embryos (Charles River). Neurons were grown on coverslips for 10–11 days *in vitro* and transfected using calcium-phosphate gene delivery (Promega), followed by fixation in 4% paraformaldehyde and analysis by immunostaining, as described below. All expression plasmids were amplified in DH5α bacteria (New England Biolabs). TDP-43 constructs (cloned into pcDNA 5T0 vector) containing mutations in nuclear localization sequences (NLSs) and acetylation-mimic Lys → Gln mutations were described previously (4). FMRP–GFP constructs containing the human FMR1 promoter were kindly provided by Dr. Jennifer Darnell (Rockefeller University). Plasmids were transfected into QBI-293 using FuGENE 6 (Promega) following the manufacturer's instructions. The cells were cultured in 6-well plates or on poly-D-lysine–coated coverslips for 24 h prior to transfection. Co-transfection of multiple plasmids (*e.g.* TDP-43–ΔNLS–K145Q combined with control vector or FMRP–GFP) was performed using FuGENE 6 per the manufacturer's protocols. Tubastatin A (TBST) was purchased from Sigma and used in cell culture experiments at a final concentration of 5 μM.

Fractionation and biochemical analysis

Biochemical analyses for preparation of cell lysates were performed similar to that previously described (4). Cells from 6-well culture dishes were sonicated and homogenized in RIPA buffer (50 mM Tris pH 8.0, 150 mM NaCl, 1% Nonidet P-40, 5 mM EDTA, 0.5% sodium deoxycholate, 0.1% SDS) supplemented with 1 mM phenylmethylsulfonyl fluoride, a mixture of protease inhibitors (1 mg ml^{-1} pepstatin, leuptin, *N*-*p*-tosyl-L-phenylalanine chloromethyl ketone, N^{α}-tosyl-L-lysine chloromethyl ketone hydrochloride, trypsin inhibitor; Sigma) and a mixture of phosphatase inhibitors (2 mM imidazole, 1 mM NaF, 1 mM sodium orthovanadate; Sigma). Lysates were then sonicated and centrifuged at 21,100 × *g* for 30 min at 4 °C and then rinsed in RIPA buffer to deplete the soluble protein pool. The insoluble pelleted fractions were then extracted in 75 μl of urea buffer (7 M urea, 2 M thiourea, 4% CHAPS, 30 mM Tris, pH 8.5), sonicated, and centrifuged at 21,100 × *g* for 30 min at room temperature.

All soluble and insoluble fractions were subsequently analyzed by immunoblotting using the following antibodies: rabbit polyclonal anti-TDP-43 (Proteintech, 10782-2-AP), rabbit polyclonal anti–phospho-TDP-43 (Ser-409/410; Proteintech, 22309-1-AP), anti-acetylated tubulin (Sigma, clone 6-11B-1), anti-α-tubulin (Sigma, clone DM1A), and anti-GAPDH (Millipore, ABS16). Dilution ratios were 1:1000 for all the antibodies unless otherwise stated. Western blotting protein band quantification was measured by densitometry using ImageQuant TL 1D, version 8.1 software (GE Healthcare Life Sciences).

For phosphatase reactions, immunoprecipitated FMRP complexes were collected on protein A/G beads and washed four times (50 mM Tris-HCl, pH 7.4, 250 mM NaCl, 5 mM EDTA, 0.1% Nonidet P-40), followed by a final wash (50 mM Tris-HCl, pH 7.5, 0.1 mM Na_2EDTA, 5 mM DTT, 2 mM $MnCl_2$). After the last wash, the pellet was divided, and half was treated with λ-phosphatase (New England Biolabs). Samples were incubated

Figure 5. Cytoplasmic FMRP granules sequester HDAC6 and enhance TDP-43 aggregation. *A*, FMRP–GFP expressing cells were double-labeled to show co-localization between FMRP granules (*green*) and endogenous HDAC6 (*red*). *Cyan arrowheads* highlight FMRP granules that recruited HDAC6. *Scale bar*, 20 μm. *B*, QBI-293 cells co-expressing cytoplasmic TDP-43 (TDP-43–ΔNLS) in the presence or absence of FMRP–GFP were treated with the HDAC6-specific inhibitor tubastatin A (TBST) (5 μM for 12 h). Cell lysates were sequentially extracted to generate soluble (RIPA-extracted) and insoluble (UREA-extracted) fractions followed by immunoblotting with TDP-43 and GAPDH antibodies. Myc-tagged TDP-43 was distinguished from endogenous TDP-43 (*end. TDP-43*) based on their distinct molecular weight differences. *C*, protein band intensities were quantified using ImageQuant TL software (version 8.1), and the values were represented as relative intensities normalized to the GAPDH loading control. *D* and *E*, cells co-expressing TDP-43–ΔNLS–2KQ and FMRP–GFP were treated with TBST, where indicated, and triple-labeled to detect FMRP (*green*), total Myc-tagged TDP-43 (*red*), and P-409/410 (*blue*). The number of inclusions and average inclusion size per cell were measured using ImageJ software and plotted in *E*. *F*, QBI-293 cells co-expressing aggregate-prone TDP-43–ΔNLS–2KQ and FMRP–GFP along with either control vector (pcDNA3.1, *lanes 1–3*), WT HDAC6 (*lanes 4–6*), HDAC6-ΔBUZ lacking residues 1045–1215 (*lanes 7–9*), or HDAC6 1–840 lacking residues 841–1215 (*lanes 10–12*) were extracted, analyzed by immunoblotting, and quantified by densitometry in *G*. All HDAC6 constructs were functional, as determined by deacetylation of tubulin. *Error bars* indicate S.E., and *p* values were calculated by Student's *t* test. ***, $p < 0.001$; **, $p < 0.01$; *, $p < 0.05$. Ectopic expression of FMRP–GFP or inhibition of HDAC6 increased TDP-43 aggregation while restoring HDAC6 expression suppressed TDP-43 aggregation. *ns*, not significant.

at 37 °C for 30 min and then collected by centrifugation. FMRP phosphorylation was assayed by immunoblotting with a P-FMRP antibody (Ser-499; PhosphoSolutions, p1125-499).

Immunocytochemistry and quantification

QBI-293 cells were grown on PDL-coated coverslips and transfected as described above and cultured for the indicated times. The cells were irreversibly fixed in 4% paraformaldehyde for 10 min, rinsed in PBS (three times), and permeabilized once with 0.2% Triton X-100 (Sigma) in PBS for 10 min. Fixed cells were then blocked in 2% milk for 1 h and incubated with specified primary antibodies overnight at 4 °C. The cells were washed in PBS and incubated with Alexa 488– or 594–conjugated secondary antibody. The nuclei were counterstained with 4′,6′-diamino-2-phenylindole (Sigma). The cells were analyzed using Metamorph software on a LSM780 confocal laser microscope (Carl Zeiss) or an Olympus IX71 microscope (Olympus).

The total number of FMRP granules in transfected cells that co-localized with ectopic TDP-43 was quantified from 8–10 fields and reported as percentage of co-localizing FMRP granules/total FMRP granules per field. FMRP granules were either endogenously produced by exposure to arsenite stress (0.5 mM, 1 h) or ectopically produced by expression of FMRP–GFP. Quantification of inclusion size, with or without TBST treatment, was performed by counting inclusion number or by measuring inclusion circumference (as determined by anti–phospho-TDP-43 staining, Ser-409/410). Average inclusion size per cell was represented relative to control conditions. The data were represented as means ± S.E. Statistical analysis was performed with a two-tailed unpaired *t* test with equal variance (significance set at p value < 0.05 (*), p value < 0.01 (**), and p value < 0.001 (***). All of the quantitative immunofluorescence analyses were independently validated and confirmed from at least three biological replicates.

Primary antibodies used for immunofluorescence and histology methods (described below) were as follows: anti-GFP (FL, Santa Cruz), anti-GFP (B2, Santa Cruz), anti–TDP-43 (Proteintech, 10782-2-AP), anti–phospho-TDP-43 (Ser-409/410; Proteintech, 22309-1-AP), anti–phospho-TDP-43 (Ser-409/410; Millipore, clone 1D3, MABN14), anti–TDP-43 C-terminal (1038) (5), anti–TDP-43 N-terminal (1065) (5), anti-FMRP (BD Transduction Laboratories, 610352), anti–phospho-FMRP (Ser-499; PhosphoSolutions, p1125–499), anti-TIAR (Millipore, MAB2160), anti-TIA1 (Santa Cruz, clone C-20), anti-Hsp70 (Enzo Life Science, SPA-810), anti-HDAC6 (Santa Cruz, clone H-300). Antibody dilutions ranged from 1:250 to 1:1000 for all antibodies unless otherwise noted.

Histology of ALS spinal cord

Lumbar spinal cord sections from a panel of ALS cases that were positive for acetylated TDP-43 inclusions (4) and were kindly provided by Dr. John Q. Trojanowski (University of Pennsylvania). Double-labeling immunofluorescence staining was performed at the University of North Carolina Translational Pathology Laboratory using the above described FMRP, P-FMRP, TIA-1, TIAR, or phospho-TDP-43 (clone 1D3) antibodies. Slides were dewaxed in Bond Dewax solution (Leica Biosystems) and hydrated in Bond Wash solution (Leica Biosystems). Antigen retrieval for both stains were done for 30 min in Bond-epitope retrieval solution 1 (pH 6.0, Leica Biosystems), followed with 5 min of endogenous peroxidase blocking with Bond peroxide blocking solution (Leica Biosystems). The protein blocking reagent (Leica Biosystems) was added for 10 min. Primary antibodies were applied for 1 h. For dual-color immunofluorescence staining, first phospho–TDP-43 was detected with rabbit anti-rat IgG (Vector labs), bond polymer (Leica Biosystems), and tyramide Cy5 (PerkinElmer Life Sciences) and then with SG markers using bond polymer and tyramide Cy3 (PerkinElmer Life Sciences). After completion of the first stain and before addition of the second primary antibody, the appropriate antigen retrieval protocol and peroxide blocking steps as described above were applied. The slides were counterstained with Hoechst (Invitrogen) and mounted with ProLong Gold antifade reagent (Life Technologies). IHC stained slides were digitally imaged in Aperio ScanScope XT (Leica Biosystems) using 20× objective. High resolution acquisition of double-color immunofluorescence slides in the 4′,6′-diamino-2-phenylindole, Cy3 and Cy5 channels was performed in Aperio ScanScope FL (Leica Biosystems) using 20× objective.

Author contributions—Y. C. data curation; Y. C. formal analysis; Y. C. methodology; T. J. C. conceptualization; T. J. C. supervision; T. J. C. investigation; T. J. C. writing-original draft; T. J. C. project administration; T. J. C. writing-review and editing.

Acknowledgments—We thank Dr. John Trojanowski and Dr. Virginia Lee (University of Pennsylvania) for providing ALS spinal cord and polyclonal TDP-43 antibodies. We thank Dr. Jennifer Darnell (Rockefeller University) for providing FMRP–GFP constructs for de novo stress granule formation. We thank Dr. Jui-Heng Tseng for technical assistance in generating primary neuronal cultures. We also thank the University of North Carolina Translational Pathology Laboratory and the University of North Carolina Animal Histopathology Core for technical support (University of North Carolina–Chapel Hill).

References

1. Neumann, M., Sampathu, D. M., Kwong, L. K., Truax, A. C., Micsenyi, M. C., Chou, T. T., Bruce, J., Schuck, T., Grossman, M., Clark, C. M., McCluskey, L. F., Miller, B. L., Masliah, E., Mackenzie, I. R., *et al.* (2006) Ubiquitinated TDP-43 in frontotemporal lobar degeneration and amyotrophic lateral sclerosis. *Science* **314,** 130–133 CrossRef Medline
2. Lagier-Tourenne, C., and Cleveland, D. W. (2009) Rethinking ALS: the FUS about TDP-43. *Cell* **136,** 1001–1004 CrossRef Medline
3. Pesiridis, G. S., Lee, V. M., and Trojanowski, J. Q. (2009) Mutations in TDP-43 link glycine-rich domain functions to amyotrophic lateral sclerosis. *Hum. Mol. Genet.* **18,** R156–R162 CrossRef Medline
4. Cohen, T. J., Hwang, A. W., Restrepo, C. R., Yuan, C. X., Trojanowski, J. Q., and Lee, V. M. (2015) An acetylation switch controls TDP-43 function and aggregation propensity. *Nat. Commun.* **6,** 5845 CrossRef Medline
5. Igaz, L. M., Kwong, L. K., Xu, Y., Truax, A. C., Uryu, K., Neumann, M., Clark, C. M., Elman, L. B., Miller, B. L., Grossman, M., McCluskey, L. F., Trojanowski, J. Q., and Lee, V. M. (2008) Enrichment of C-terminal fragments in TAR DNA-binding protein-43 cytoplasmic inclusions in brain but not in spinal cord of frontotemporal lobar degeneration and amyotrophic lateral sclerosis. *Am. J. Pathol.* **173,** 182–194 CrossRef Medline
6. Kametani, F., Obi, T., Shishido, T., Akatsu, H., Murayama, S., Saito, Y., Yoshida, M., and Hasegawa, M. (2016) Mass spectrometric analysis of accumulated TDP-43 in amyotrophic lateral sclerosis brains. *Sci. Rep.* **6,** 23281 CrossRef Medline

7. Valle, C., and Carrì, M. T. (2017) Cysteine modifications in the pathogenesis of ALS. *Front. Mol. Neurosci.* **10,** 5 Medline
8. Li, H. Y., Yeh, P. A., Chiu, H. C., Tang, C. Y., and Tu, B. P. (2011) Hyperphosphorylation as a defense mechanism to reduce TDP-43 aggregation. *PLoS One* **6,** e23075 CrossRef Medline
9. Wang, P., Wander, C. M., Yuan, C. X., Bereman, M. S., and Cohen, T. J. (2017) Acetylation-induced TDP-43 pathology is suppressed by an HSF1-dependent chaperone program. *Nat. Commun.* **8,** 82 CrossRef Medline
10. Neumann, M., Kwong, L. K., Lee, E. B., Kremmer, E., Flatley, A., Xu, Y., Forman, M. S., Troost, D., Kretzschmar, H. A., Trojanowski, J. Q., and Lee, V. M. (2009) Phosphorylation of S409/410 of TDP-43 is a consistent feature in all sporadic and familial forms of TDP-43 proteinopathies. *Acta Neuropathol.* **117,** 137–149 CrossRef Medline
11. Bhandare, V. V., and Ramaswamy, A. (2017) The proteinopathy of D169G and K263E mutants at the RNA recognition motif (RRM) domain of tar DNA-binding protein (tdp43) causing neurological disorders: a computational study. *J. Biomol. Struct. Dyn.* **36,** 1075–1093 CrossRef Medline
12. Moreno, F., Rabinovici, G. D., Karydas, A., Miller, Z., Hsu, S. C., Legati, A., Fong, J., Schonhaut, D., Esselmann, H., Watson, C., Stephens, M. L., Kramer, J., Wiltfang, J., Seeley, W. W., Miller, B. L., *et al.* (2015) A novel mutation P112H in the TARDBP gene associated with frontotemporal lobar degeneration without motor neuron disease and abundant neuritic amyloid plaques. *Acta Neuropathol. Commun.* **3,** 19 CrossRef Medline
13. Anderson, P., and Kedersha, N. (2008) Stress granules: the Tao of RNA triage. *Trends Biochem. Sci.* **33,** 141–150 CrossRef Medline
14. Anderson, P., and Kedersha, N. (2009) RNA granules: post-transcriptional and epigenetic modulators of gene expression. *Nat. Rev. Mol. Cell Biol.* **10,** 430–436 CrossRef Medline
15. Colombrita, C., Zennaro, E., Fallini, C., Weber, M., Sommacal, A., Buratti, E., Silani, V., and Ratti, A. (2009) TDP-43 is recruited to stress granules in conditions of oxidative insult. *J. Neurochem.* **111,** 1051–1061 CrossRef Medline
16. Dewey, C. M., Cenik, B., Sephton, C. F., Dries, D. R., Mayer, P., 3rd, Good, S. K., Johnson, B. A., Herz, J., and Yu, G. (2011) TDP-43 is directed to stress granules by sorbitol, a novel physiological osmotic and oxidative stressor. *Mol. Cell. Biol.* **31,** 1098–1108 CrossRef Medline
17. Freibaum, B. D., Chitta, R. K., High, A. A., and Taylor, J. P. (2010) Global analysis of TDP-43 interacting proteins reveals strong association with RNA splicing and translation machinery. *J. Proteome Res.* **9,** 1104–1120 CrossRef Medline
18. Liu-Yesucevitz, L., Bilgutay, A., Zhang, Y. J., Vanderweyde, T., Citro, A., Mehta, T., Zaarur, N., McKee, A., Bowser, R., Sherman, M., Petrucelli, L., and Wolozin, B. (2010) Tar DNA binding protein-43 (TDP-43) associates with stress granules: analysis of cultured cells and pathological brain tissue. *PLoS One* **5,** e13250 CrossRef Medline
19. McDonald, K. K., Aulas, A., Destroismaisons, L., Pickles, S., Beleac, E., Camu, W., Rouleau, G. A., and Vande Velde, C. (2011) TAR DNA-binding protein 43 (TDP-43) regulates stress granule dynamics via differential regulation of G3BP and TIA-1. *Hum. Mol. Genet.* **20,** 1400–1410 CrossRef Medline
20. Nishimoto, Y., Ito, D., Yagi, T., Nihei, Y., Tsunoda, Y., and Suzuki, N. (2010) Characterization of alternative isoforms and inclusion body of the TAR DNA-binding protein-43. *J. Biol. Chem.* **285,** 608–619 CrossRef Medline
21. Cohen, T. J., Hwang, A. W., Unger, T., Trojanowski, J. Q., and Lee, V. M. (2012) Redox signalling directly regulates TDP-43 via cysteine oxidation and disulphide cross-linking. *EMBO J.* **31,** 1241–1252 CrossRef Medline
22. Aulas, A., and Vande Velde, C. (2015) Alterations in stress granule dynamics driven by TDP-43 and FUS: a link to pathological inclusions in ALS? *Front. Cell Neurosci.* **9,** 423 Medline
23. Li, Y. R., King, O. D., Shorter, J., and Gitler, A. D. (2013) Stress granules as crucibles of ALS pathogenesis. *J. Cell Biol.* **201,** 361–372 CrossRef Medline
24. Monahan, Z., Shewmaker, F., and Pandey, U. B. (2016) Stress granules at the intersection of autophagy and ALS. *Brain Res.* **1649,** 189–200 CrossRef Medline
25. Coyne, A. N., Yamada, S. B., Siddegowda, B. B., Estes, P. S., Zaepfel, B. L., Johannesmeyer, J. S., Lockwood, D. B., Pham, L. T., Hart, M. P., Cassel, J. A., Freibaum, B., Boehringer, A. V., Taylor, J. P., Reitz, A. B., Gitler, A. D., *et al.* (2015) Fragile X protein mitigates TDP-43 toxicity by remodeling RNA granules and restoring translation. *Hum. Mol. Genet.* **24,** 6886–6898 Medline
26. Liu-Yesucevitz, L., Bassell, G. J., Gitler, A. D., Hart, A. C., Klann, E., Richter, J. D., Warren, S. T., and Wolozin, B. (2011) Local RNA translation at the synapse and in disease. *J. Neurosci.* **31,** 16086–16093 CrossRef Medline
27. Majumder, P., Chu, J. F., Chatterjee, B., Swamy, K. B., and Shen, C. J. (2016) Co-regulation of mRNA translation by TDP-43 and Fragile X Syndrome protein FMRP. *Acta Neuropathol.* **132,** 721–738 CrossRef Medline
28. Yu, Z., Fan, D., Gui, B., Shi, L., Xuan, C., Shan, L., Wang, Q., Shang, Y., and Wang, Y. (2012) Neurodegeneration-associated TDP-43 interacts with fragile X mental retardation protein (FMRP)/Staufen (STAU1) and regulates SIRT1 expression in neuronal cells. *J. Biol. Chem.* **287,** 22560–22572 CrossRef Medline
29. Liu-Yesucevitz, L., Bilgutay, A., Zhang, Y. J., Vanderweyde, T., Citro, A., Mehta, T., Zaarur, N., McKee, A., Bowser, R., Sherman, M., Petrucelli, L., and Wolozin, B. (2010) Tar DNA binding protein-43 (TDP-43) associates with stress granules: analysis of cultured cells and pathological brain tissue. *PLoS One* **5,** e13250 CrossRef Medline
30. Darnell, J. C., Mostovetsky, O., and Darnell, R. B. (2005) FMRP RNA targets: identification and validation. *Genes Brain Behav.* **4,** 341–349 CrossRef Medline
31. Mazroui, R., Huot, M. E., Tremblay, S., Boilard, N., Labelle, Y., and Khandjian, E. W. (2003) Fragile X mental retardation protein determinants required for its association with polyribosomal mRNPs. *Hum. Mol. Genet.* **12,** 3087–3096 CrossRef Medline
32. Mazroui, R., Huot, M. E., Tremblay, S., Filion, C., Labelle, Y., and Khandjian, E. W. (2002) Trapping of messenger RNA by fragile X mental retardation protein into cytoplasmic granules induces translation repression. *Hum. Mol. Genet.* **11,** 3007–3017 CrossRef Medline
33. Ceman, S., O'Donnell, W. T., Reed, M., Patton, S., Pohl, J., and Warren, S. T. (2003) Phosphorylation influences the translation state of FMRP-associated polyribosomes. *Hum. Mol. Genet.* **12,** 3295–3305 CrossRef Medline
34. Kwon, S., Zhang, Y., and Matthias, P. (2007) The deacetylase HDAC6 is a novel critical component of stress granules involved in the stress response. *Genes Dev.* **21,** 3381–3394 CrossRef Medline
35. Kawaguchi, Y., Kovacs, J. J., McLaurin, A., Vance, J. M., Ito, A., and Yao, T. P. (2003) The deacetylase HDAC6 regulates aggresome formation and cell viability in response to misfolded protein stress. *Cell* **115,** 727–738 CrossRef Medline
36. Lee, J. Y., Koga, H., Kawaguchi, Y., Tang, W., Wong, E., Gao, Y. S., Pandey, U. B., Kaushik, S., Tresse, E., Lu, J., Taylor, J. P., Cuervo, A. M., and Yao, T. P. (2010) HDAC6 controls autophagosome maturation essential for ubiquitin-selective quality-control autophagy. *EMBO J.* **29,** 969–980 CrossRef Medline
37. Iwata, A., Riley, B. E., Johnston, J. A., and Kopito, R. R. (2005) HDAC6 and microtubules are required for autophagic degradation of aggregated huntingtin. *J. Biol. Chem.* **280,** 40282–40292 CrossRef Medline
38. Pandey, U. B., Nie, Z., Batlevi, Y., McCray, B. A., Ritson, G. P., Nedelsky, N. B., Schwartz, S. L., DiProspero, N. A., Knight, M. A., Schuldiner, O., Padmanabhan, R., Hild, M., Berry, D. L., Garza, D., Hubbert, C. C., *et al.* (2007) HDAC6 rescues neurodegeneration and provides an essential link between autophagy and the UPS. *Nature* **447,** 859–863 Medline
39. Ding, H., Dolan, P. J., and Johnson, G. V. (2008) Histone deacetylase 6 interacts with the microtubule-associated protein tau. *J. Neurochem.* **106,** 2119–2130 CrossRef Medline
40. Gal, J., Chen, J., Barnett, K. R., Yang, L., Brumley, E., and Zhu, H. (2013) HDAC6 regulates mutant SOD1 aggregation through two SMIR motifs and tubulin acetylation. *J. Biol. Chem.* **288,** 15035–15045 CrossRef Medline
41. Cohen, T. J., Lee, V. M., and Trojanowski, J. Q. (2011) TDP-43 functions and pathogenic mechanisms implicated in TDP-43 proteinopathies. *Trends Mol. Med.* **17,** 659–667 CrossRef Medline
42. Shelkovnikova, T. A., Robinson, H. K., Southcombe, J. A., Ninkina, N., and Buchman, V. L. (2014) Multistep process of FUS aggregation in the cell

cytoplasm involves RNA-dependent and RNA-independent mechanisms. *Hum. Mol. Genet.* **23,** 5211–5226 CrossRef Medline

43. Gopal, P. P., Nirschl, J. J., Klinman, E., and Holzbaur, E. L. (2017) Amyotrophic lateral sclerosis-linked mutations increase the viscosity of liquid-like TDP-43 RNP granules in neurons. *Proc. Natl. Acad. Sci. U.S.A.* **114,** E2466–E2475 CrossRef Medline
44. Molliex, A., Temirov, J., Lee, J., Coughlin, M., Kanagaraj, A. P., Kim, H. J., Mittag, T., and Taylor, J. P. (2015) Phase separation by low complexity domains promotes stress granule assembly and drives pathological fibrillization. *Cell* **163,** 123–133 CrossRef Medline
45. Murakami, T., Qamar, S., Lin, J. Q., Schierle, G. S., Rees, E., Miyashita, A., Costa, A. R., Dodd, R. B., Chan, F. T., Michel, C. H., Kronenberg-Versteeg, D., Li, Y., Yang, S. P., Wakutani, Y., Meadows, W., *et al.* (2015) ALS/FTD mutation-induced phase transition of FUS liquid droplets and reversible hydrogels into irreversible hydrogels impairs RNP granule function. *Neuron* **88,** 678–690 CrossRef Medline
46. Patel, A., Lee, H. O., Jawerth, L., Maharana, S., Jahnel, M., Hein, M. Y., Stoynov, S., Mahamid, J., Saha, S., Franzmann, T. M., Pozniakovski, A., Poser, I., Maghelli, N., Royer, L. A., Weigert, M., *et al.* (2015) A liquid-to-solid phase transition of the ALS protein FUS accelerated by disease mutation. *Cell* **162,** 1066–1077 CrossRef Medline
47. McGurk, L., Gomes, E., Guo, L., Mojsilovic-Petrovic, J., Tran, V., Kalb, R. G., Shorter, J., and Bonini, N. M. (2018) Poly(ADP-ribose) prevents pathological phase separation of TDP-43 by promoting liquid demixing and stress granule localization. *Mol. Cell* **71,** 703–717.e9 CrossRef Medline
48. Hirsch-Reinshagen, V., Pottier, C., Nicholson, A. M., Baker, M., Hsiung, G. R., Krieger, C., Sengdy, P., Boylan, K. B., Dickson, D. W., Mesulam, M., Weintraub, S., Bigio, E., Zinman, L., Keith, J., Rogaeva, E., *et al.* (2017) Clinical and neuropathological features of ALS/FTD with TIA1 mutations. *Acta Neuropathol. Commun.* **5,** 96 CrossRef Medline
49. Mackenzie, I. R., Nicholson, A. M., Sarkar, M., Messing, J., Purice, M. D., Pottier, C., Annu, K., Baker, M., Perkerson, R. B., Kurti, A., Matchett, B. J., Mittag, T., Temirov, J., Hsiung, G. R., Krieger, C., *et al.* (2017) TIA1 mutations in amyotrophic lateral sclerosis and frontotemporal dementia promote phase separation and alter stress granule dynamics. *Neuron* **95,** 808–816.e9 CrossRef Medline
50. Guo, W., Naujock, M., Fumagalli, L., Vandoorne, T., Baatsen, P., Boon, R., Ordovás, L., Patel, A., Welters, M., Vanwelden, T., Geens, N., Tricot, T., Benoy, V., Steyaert, J., Lefebvre-Omar, C., *et al.* (2017) HDAC6 inhibition reverses axonal transport defects in motor neurons derived from FUS-ALS patients. *Nat. Commun.* **8,** 861 CrossRef Medline
51. Taes, I., Timmers, M., Hersmus, N., Bento-Abreu, A., Van Den Bosch, L., Van Damme, P., Auwerx, J., and Robberecht, W. (2013) Hdac6 deletion delays disease progression in the SOD1G93A mouse model of ALS. *Hum. Mol. Genet.* **22,** 1783–1790 CrossRef Medline
52. Lee, J. Y., Nagano, Y., Taylor, J. P., Lim, K. L., and Yao, T. P. (2010) Disease-causing mutations in parkin impair mitochondrial ubiquitination, aggregation, and HDAC6-dependent mitophagy. *J. Cell Biol.* **189,** 671–679 CrossRef Medline
53. Zhang, X., Yuan, Z., Zhang, Y., Yong, S., Salas-Burgos, A., Koomen, J., Olashaw, N., Parsons, J. T., Yang, X. J., Dent, S. R., Yao, T. P., Lane, W. S., and Seto, E. (2007) HDAC6 modulates cell motility by altering the acetylation level of cortactin. *Mol. Cell* **27,** 197–213 CrossRef Medline
54. Hwang, A. W., Trzeciakiewicz, H., Friedmann, D., Yuan, C. X., Marmorstein, R., Lee, V. M., and Cohen, T. J. (2016) Conserved lysine acetylation within the microtubule-binding domain regulates MAP2/Tau family members. *PLoS One* **11,** e0168913 CrossRef Medline
55. Kovacs, J. J., Murphy, P. J., Gaillard, S., Zhao, X., Wu, J. T., Nicchitta, C. V., Yoshida, M., Toft, D. O., Pratt, W. B., and Yao, T. P. (2005) HDAC6 regulates Hsp90 acetylation and chaperone-dependent activation of glucocorticoid receptor. *Mol. Cell* **18,** 601–607 CrossRef Medline
56. Zhang, L., Liu, S., Liu, N., Zhang, Y., Liu, M., Li, D., Seto, E., Yao, T. P., Shui, W., and Zhou, J. (2015) Proteomic identification and functional characterization of MYH9, Hsc70, and DNAJA1 as novel substrates of HDAC6 deacetylase activity. *Protein Cell* **6,** 42–54 CrossRef Medline